J. Chem. Sci. (2019) 131:98
https://doi.org/10.1007/s12039-019-1674-x

REGULAR ARTICLE

Special Issue on Materials Chemistry

Hydrogen storage properties of Ti_2FeV BCC solid solution

TAPAS KUMAR DAS[a,b], ASHEESH KUMAR[a], PRIYANKA RUZ[a], SEEMITA BANERJEE[a,c,*] and V SUDARSAN[a,c,*]

[a]Chemistry Division Bhabha Atomic Research Centre, Mumbai 400 085, Maharashtra, India
[b]UM-DAE-Centre for Excellence in Basic Sciences, Health Centre, Mumbai University, Kalina Campus, Mumbai 400 098, Maharashtra, India
[c]Homi Bhabha National Institute, Mumbai 400 094, Maharashtra, India
E-mail: seemita@barc.gov.in; vsudar@barc.gov.in

MS received 17 April 2019; revised 14 July 2019; accepted 18 July 2019; published online 14 October 2019

Abstract. This paper deals with hydrogen storage properties of Ti-V based BCC solid solution incorporated with Fe. The alloy with composition Ti_2FeV was prepared by arc melting method. X-ray diffraction (XRD) and energy dispersive X-ray analysis studies confirmed formation of solid solution phase with uniform composition and BCC structure. SEM studies revealed the formation of irregular shaped particles with size in the range of few microns up on hydrogenation of the parent alloy. The alloy shows maximum hydrogen storage capacity of 3.41 wt.% at 20 bar and 303 K and the thermodynamic parameters established near room temperature suitability of the alloy for solid state hydrogen storage applications. Hydrogenation kinetics is found to be quite fast and detailed kinetic analysis were done to underscore the hydrogenation mechanism. Activation energy during the initial stage of hydrogenation is found to be 30.8 kJ/mol. The value decreases to 14.4 kJ/mol for extended duration of hydrogenation, and this is explained based on difference in rate determining steps existing at different time scales.

Keywords. Ti-V alloy; BCC solid solution; hydrogen storage; kinetics.

1. Introduction

In search of alternative energy sources to fossil fuels, considerable attention has been given to the development of different types of alloys which can reversibly absorb large amount of hydrogen and thus can be used as potential hydrogen storage material. The development of high performance hydrogen storage alloys is crucial for the establishment of renewable and clean hydrogen energy based economy.[1,2] Various types of hydrogen storage alloys have been studied and these are mainly categorized as AB, AB_5, AB_3, A_2B_7, AB_2 type Laves phase alloys, and Mg-based alloys.[3–7] In addition to this, Ti-V based BCC solid solutions are very promising candidates for practical hydrogen storage applications because of their higher hydrogen storage capacity.[8,9] However, these alloys are identified with some noticeable shortcomings such as very low desorption capacity and difficulty in activation.[10] In an attempt to improve the overall performance of these alloys, the effect of additives such as Cr, Mn, and Fe has been studied.[11–14] Based on earlier studies on Ti-Nb-Fe based alloys,[15] it is expected that addition of Fe (in a controlled quantity) into Ti-V based alloy system can improve its hydrogen storage properties.[15] Moreover, partial substitution of expensive V metal by less costlier Fe reduces the overall cost of the alloy. As an initial attempt, the concentration of Ti metal has been maintained relatively high while fixing the Fe/V ratio as 1.

In the present study, Ti_2FeV alloy has been prepared by arc melting method and its hydrogen storage properties have been evaluated as a function of temperature. Thermodynamic and kinetic aspects of hydrogen absorption by this alloy have been discussed in detail in the paper. To the best of the authors' knowledge this is the first time that a detailed investigation is reported on hydrogen storage properties of Fe incorporated Ti-V based alloy.

2. Experimental

The alloy Ti_2FeV was prepared by arc-melting highly pure (>99.99%) Ti, V and Fe metal in a Zr gettered argon atmosphere using tungsten electrode. It was re-

*For correspondence

melted four times to ensure homogeneity of the alloy composition. Phase structure of the alloy was determined by X-ray diffraction technique (Philips PW1710). XRD pattern was recorded using monochromatic CuK_α radiation. Analysis of elemental composition of the as-prepared alloy was performed using an Energy Dispersive X-ray Spectrometer (Oxford instrument Inc, UK made, Model INCA E350). Electron energy of 20 keV was used for energy dispersive spectroscopic (EDS) analysis.

Pressure-composition absorption desorption isotherms (PCI) of the alloy were measured using an automated Sievert's type setup (Hiden Isochema, UK). Around 1 g of the alloy sample was loaded into a gold-coated copper reactor and was evacuated with the help of a turbomolecular vacuum pump. The sample was activated under vacuum ($\sim 10^{-6}$ mbar, obtained using a diffusion pump) at 673 K. After 2 h of activation, sample was cooled down at working temperature under vacuum. The PCI measurements were performed at four different temperatures of 303 K, 323 K, 348 K and 373 K under a hydrogen pressure of 20 bar. Hydrogenation kinetics was carried out at 303 K, 323 K and 373 K in a home-made Sieverts type of setup under 20 bar of hydrogen pressure after one absorption–desorption cycle. The morphology of the alloy before and after hydrogenation was investigated by using a Scanning Electron Microscope (SERON INC South Korea, Model ATS 2100).

3. Results and Discussions

3.1 *XRD studies*

XRD pattern of as-prepared Ti_2FeV alloy has been presented in Figure 1. The XRD pattern confirms the formation of Ti-based BCC solid solution phase along with small amounts of oxide phase (marked by symbol "o"). The lattice parameter of the main BCC alloy phase is evaluated based on least square fitting and found to be a = 3.06 Å which is smaller than that of its chromium analogue i.e. Ti_2CrV alloy (a = 3.10 Å), reported earlier.[13] This can be explained based on smaller radius of Fe (r_{Fe} = 126 pm) compared to Cr (r_{Cr} = 128 pm). Presence of Fe_3O_4 phase (PCPDF 79-0417) is probably due to slight oxygen and moisture (<2 ppm) present in the Ar stream used for arc melting.

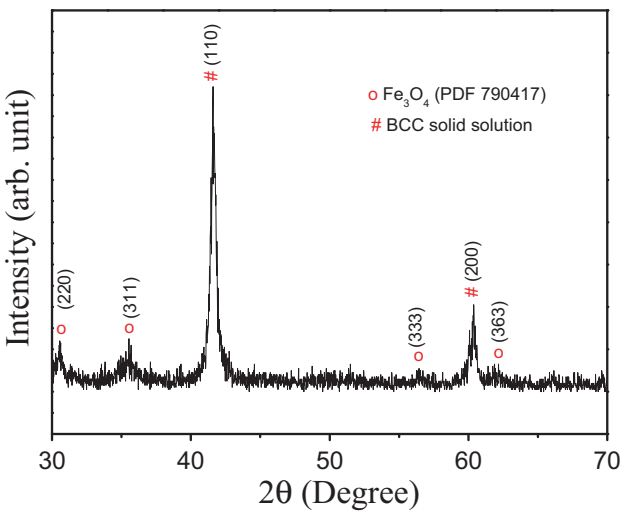

Figure 1. XRD pattern of Ti_2FeV alloy.

3.2 *Compositional analysis*

To confirm the elemental composition of as-prepared alloy, EDS analysis was performed at different positions on the alloy surface. It may be noted that the EDS technique, with electron beam energy of 20 keV, provides surface elemental composition to a depth scale of approximately 2 μm from the surface of the alloy. Figure 2 shows EDS mapping of Ti_2FeV alloy. Composition of constituent elements obtained from EDS analysis (as mentioned in Table 1) match well with those of initial amounts taken for preparing the alloy. Like XRD analysis, EDS data also reveals the presence of small amounts of oxide phase along with the Ti-based BCC solid solution.

3.3 *Hydrogen storage properties*

3.3a *Thermodynamics*: Figure 3(a) shows the characteristic pressure-composition absorption desorption isotherms (PCI) of Ti_2FeV alloy measured in the range of 303 K to 373 K. The plateau pressure is clearly visible in the absorption isotherms corresponding to 303 K, 323 K and 348 K.

However, the absorption isotherm at 373 K is too steep and it does not show any plateau pressure. The equilibrium plateau pressures (P_{eq}) at different temperatures are determined from the midpoint of absorption isotherm plateaus and are listed in Table 2. The absorption isotherm at 303 K shows an equilibrium hydrogen pressure of 1.15 bar with a storage capacity of 2.8 wt.% The absorption isotherms at 323 K and 348 K show a remarkable decrease in plateau width and the plateau disappears at 373 K as already mentioned. Generally PCI diagram of any alloy system consists of three regions namely α, α+β and β. In the α phase region, hydrogen atoms enter into the interstitial sites of the BCC alloy. With increase in hydrogen concentration, alloy is converted

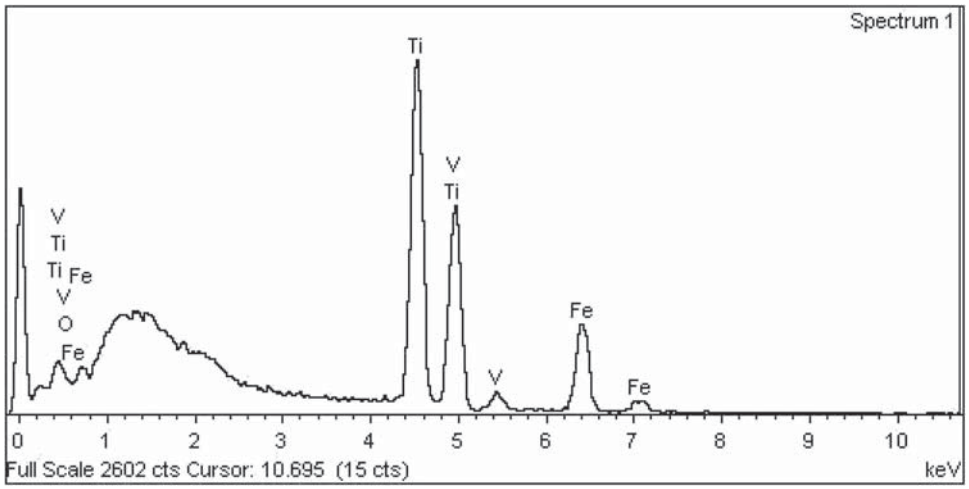

Figure 2. Representative energy dispersive X-ray spectrum of Ti_2FeV.

Table 1. Elemental composition of Ti_2FeV alloy evaluated from EDS results.

Sr. no.	Elements	Weight%	At.%
1	Ti	48.95	50.58
2	V	24.06	23.88
3	Fe	21.05	19.17
4	O	5.94	6.37

Table 2. Hydrogen storage characteristics of Ti_2FeV alloy.

Temperature (K)	P_{eq} (bar)	C_{max} (wt.%)
303	1.15	3.41
323	5.4	3.03
348	16.42	2.52

into its corresponding hydride which is called β phase. The β phase remains in equilibrium with α phase and this (α+β) mixed phase region is called plateau region. Thus, the plateau region simply corresponds to the miscibility gap, where partially immiscible α and β phases coexist. The plateau region determines the reversible hydrogen storage capacity of the alloy at that particular temperature. Mutual solubility of α and β phases increases with increase in temperature resulting in narrower plateau regions at elevated temperatures.[16] Maximum hydrogen storage capacities (C_{max}) at different temperatures for Ti_2FeV alloy are listed in Table 2. It can be seen that as expected the total hydrogen storage capacity decreases with increase in temperature.

Enthalpy change (ΔH) and entropy change (ΔS) of the alloy during hydride formation can be calculated from the absorption isotherms at different temperatures using Van't Hoff equation (equation 1).

$$\ln P_{eq} = -{}^{\Delta H}/_{RT} + {}^{\Delta S}/_{R} \quad (1)$$

where, T is the absolute temperature, R is the gas constant, and P_{eq} stands for equilibrium pressure. A plot of $\ln P_{eq}$ vs. $1000/T$ (also known as Van't Hoff

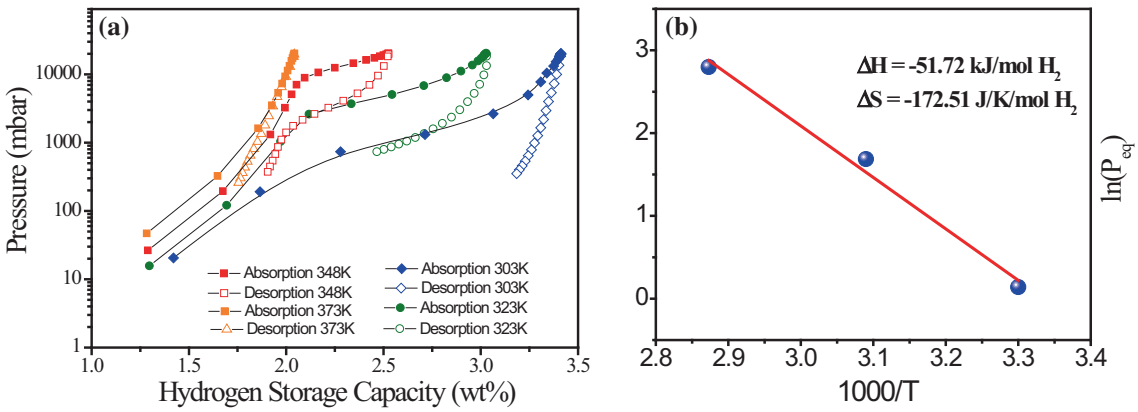

Figure 3. Hydrogen absorption–desorption isotherms (a) and Van't Hoff plot (b) of Ti_2FeV alloy.

plot) is shown in Figure 3(b). Thermodynamic parameters, ΔH and ΔS are calculated from the slope and intercept of Van't Hoff plot. Value of ΔH for Ti_2FeV alloy is found to be −51.72 kJ/mol H_2 which is lower than that involved in the hydrogenation for Ti_2CrV alloy (ΔH = −64.4 kJ/mol H_2).[12] Lower ΔH value indicates that the saturated hydride of Ti_2FeV alloy is unstable compared to its Cr analogue. As a result of this, Ti_2FeV shows a relatively higher plateau pressure compared to Ti_2CrV alloy reported earlier.[13] The BCC cell volume of Ti_2FeV alloy is lower compared to that of Ti_2CrV alloy which leads to decrease in size of H absorbing sites and reduces neighboring H–H distance and lead to rise in plateau pressure. The equilibrium plateau pressure of Ti_2FeV alloy is ∼1.15 bar at room temperature whereas that of Ti_2CrV alloy is less than 0.02 bar.[13] Thus, by changing the composition from Ti_2CrV to Ti_2FeV, equilibrium plateau pressure has been brought close to one atmosphere.

Figure 4(a and b) shows SEM images of Ti_2FeV alloy and its hydride. Hydride sample was obtained after subjecting the alloy to number of hydrogen absorption and desorption cycles. The pristine alloy shows layered texture, as can be seen from Figure 4(a). Unlike this, SEM image of hydride sample is characterized by some visible cracks on the surface. Particles observed from the SEM image of hydride sample are in the range of few microns in size as can be seen from the inset of Figure 4(b).

The cracks visible on hydride surface are generated due to hydrogen absorption desorption which leads to volume expansion and contraction respectively.

3.3b *Kinetics*: Figure 5 shows hydrogen absorption kinetics of Ti_2FeV alloy measured at 303 K, 323 K, and 373 K under isothermal conditions, where the reacted fraction (ζ) is plotted as a function of time. The reacted fraction (ζ) is defined as $(P_0 - P(t))/(P_0 - P\infty)$, where P_0, P(t) and $P\infty$ are pressures at the beginning of hydrogen absorption reaction, at reaction time t and at final equilibrium, respectively.

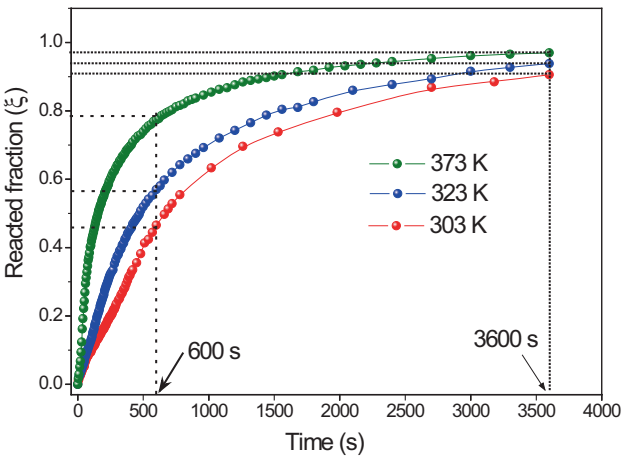

Figure 5. Hydrogen absorption kinetics of Ti_2FeV alloy at different temperatures.

Hydrogen absorption kinetics follows the same trend at all the three temperatures: relatively higher hydrogenation rate at initial stage followed by slow rate of absorption. There is a huge difference between the initial hydrogen pressure and equilibrium pressure which is responsible for the higher rate of hydrogen absorption in the beginning. With progress in reaction time, the pressure difference decreases and due to drop in driving force, rate of hydrogen absorption also decreases. The kinetics of hydrogen absorption observed at higher temperatures (323 K and 373 K) is similar to that observed at 303 K as already mentioned, but the initial rate of hydrogen absorption was faster. As shown in Figure 5, the reacted fraction (ζ) reached 0.46 within 600 s at 303 K while ζ = 0.57 and 0.78 at 323 K and 373 K, respectively after the same reaction time.

It is clearly seen from Figure 5 that the gap between the kinetic curves decreases as the reaction proceeds.

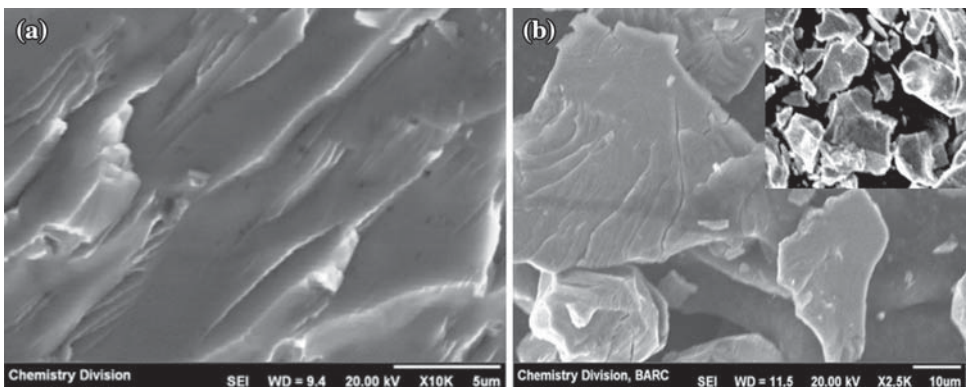

Figure 4. Representative SEM images of Ti_2FeV alloy (a) and its hydride (b).

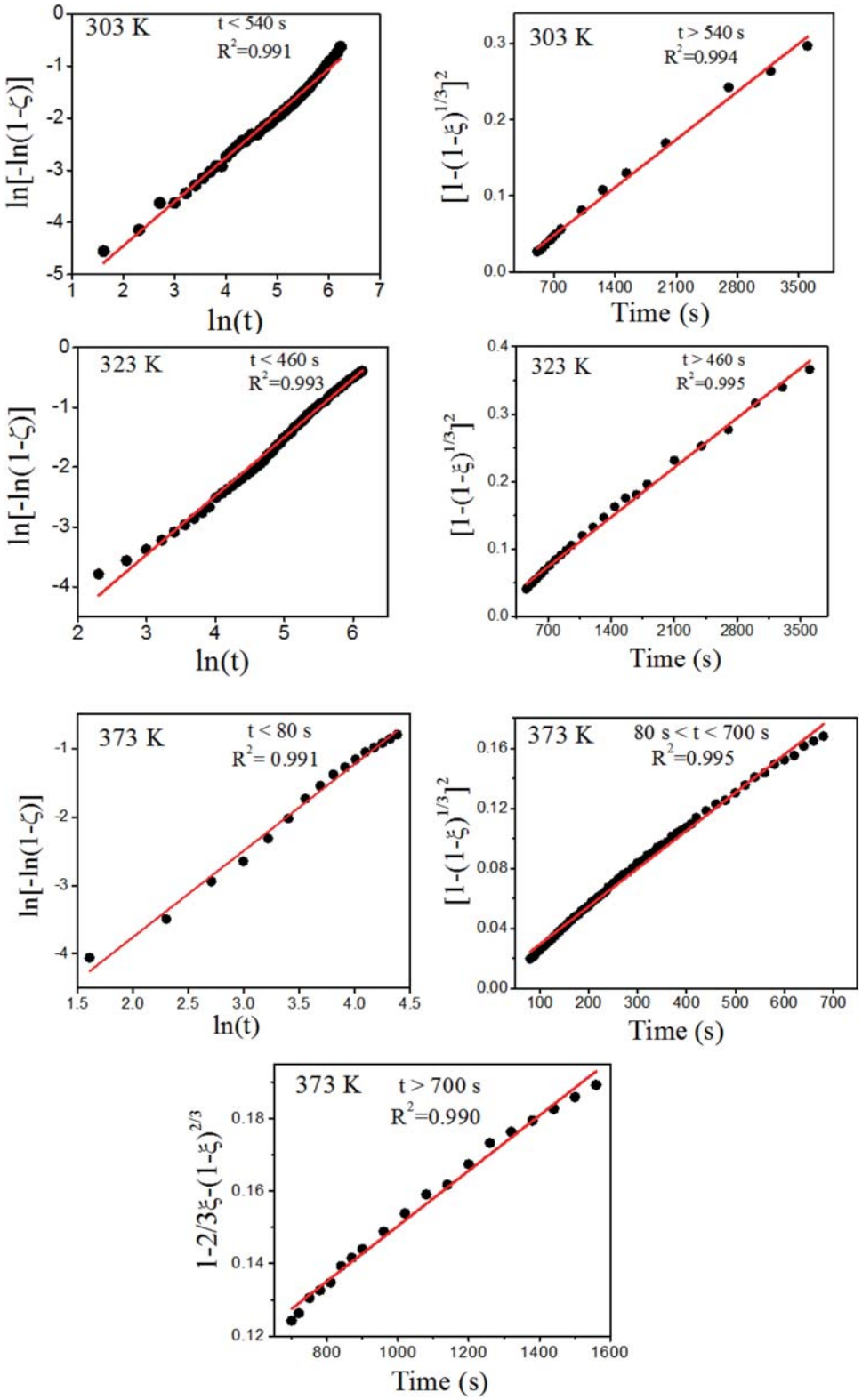

Figure 6. Fitting of hydrogen absorption kinetics of Ti_2FeV alloy with different models.

ζ = 0.91, 0.94 and 0.97 at 303 K, 323 K and 373 K, respectively at t = 3600 s.

Furthermore, the underlying mechanism of hydrogen absorption in Ti_2FeV alloy is also investigated in the present study. Generally, hydrogen absorption reaction in any metal/alloy system is expressed by the following rate equation (equation 2)

Table 3. Rate constants at different temperatures for Ti_2FeV alloy.

Stages	Best fitting kinetic model	Temperature (K)	Rate constant (k)
1	$\ln(-\ln(1-\xi)) = \text{nlnk} + \text{nln}t$	303	7.09×10^{-4}
		323	1.47×10^{-3}
		373	6.98×10^{-3}
2	$1 - {}^{2}/_{3}\xi - (1-\xi)^{2/3} = \text{kt}$	303	–
		323	–
		373	1.5×10^{-3}
3	$\left[1-(1-\xi)^{1/3}\right]^2 = \text{k}t$	303	8.99×10^{-5}
		323	1.05×10^{-4}
		373	2.53×10^{-4}

$$f(\xi) = \text{k}t \tag{2}$$

where k is the rate constant, ξ is the reacted fraction in time t and the term $f(\xi)$ is related to the reaction mechanism. The mechanism of hydrogen absorption reaction varies from system to system and various kinetic models have been proposed to interpret the reaction mechanism.[17,18] The function $f(\xi)$ giving the largest correlation coefficient (R^2) is considered as the best fitting equation to depict mechanism of hydrogen absorption in the alloy. From these equations, rate constant k can be obtained at different temperatures and subsequently activation energy can be calculated using Arrhenius equation. Thus, using this method, overall mechanism of alloy-hydrogen reaction can be predicted. However, this type of kinetic analysis based on model fitting becomes troublesome when more than one rate determining steps are involved during the progress of reaction. In the present study, it has been found that two different kinetic rate equations are required to fit whole range of kinetics data at 303 K and 323 K. Further, the kinetics data of hydrogen absorption at 373 K needs three different rate equations for explaining the reaction satisfactorily and the same is discussed in the following text.

The initial kinetics data of hydrogen absorption for all the three temperatures (303 K, 323 K and 373 K) was fitted well with Kolmogorov-Johnson-Mehl-Avrami (KJMA) model. Closeness of experimental and fitted data is reflected in the correlation coefficient values, $R^2 > 0.99$, of linear regression equations as mentioned in Figure 6. KJMA model represents random nucleation and non-directional growth of nuclei.[19] Hence, from the results of kinetics analysis it is presumed that the hydrogen absorption reaction of Ti_2FeV alloy proceeds through nucleation and growth mechanism in the beginning. However, the experimental kinetics data after initial absorption period hardly fits with KJMA model and it fits extremely well with 3D Jander diffusion model, expressed as $[1-(1-\zeta)^{1/3}]^2 = \text{kt}$, for the reaction temperatures 303 K and 323 K. The kinetics data at 373 K needs one more rate equation to fit the data in between 80 s and 700 s. This range of data is better fitted with Ginstling-Braunshtein model, another 3D diffusion model expressed as $[1-2/3\zeta-(1-\zeta)^{2/3}] = \text{kt}$. The Jander diffusion model is based on the assumption of spherical reactant surface and plane product surface, whereas the Ginstling-Brounshtein model assumes both reactant surface and product layer as spherical.[20] Carter[21] pointed out that Jander diffusion model is oversimplified and valid only for small values of reacted fraction ζ. It is also observed that Jander diffusion model cannot explain the behavior of reaction kinetics as the reaction proceeds towards completion i.e. for higher values of ζ.[22] The variation of reaction mechanism from Jander diffusion to Ginstling-Braunshtein is due to continuous change in geometry of the particles as the reaction proceeds.

The kinetic parameter k along with best fitting rate equations is mentioned in Table 3. The rate constants (k) have been evaluated using the best fitting kinetic models at three different temperatures for different stages of hydrogen absorption. The related activation energies of hydrogen absorption steps have been determined using the Arrhenius equation (equation 3).

$$\ln k = \ln \text{A} - \frac{\text{E}_\text{a}}{\text{R}T} \tag{3}$$

where, A and E_a stand for pre-exponential factor and activation energy, respectively. T is the temperature and R is the universal gas constant.

The activation energies of hydrogen absorption for Ti_2FeV alloy have been found to be 30.8 kJ/mol and 14.4 kJ/mol for nucleation & growth and Jander diffusion controlled steps, respectively and are mentioned in Figure 7. In our earlier studies, the mechanism of hydrogen absorption has also been found to involve

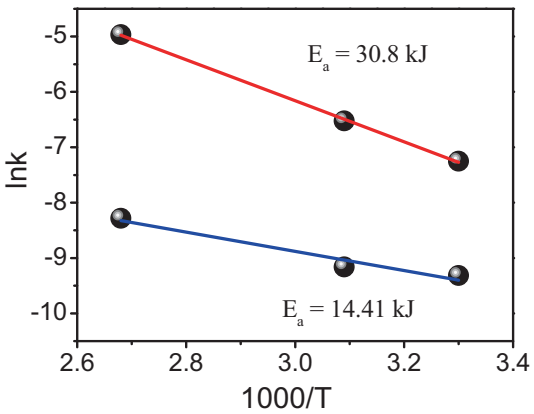

Figure 7. Activation energies of Ti_2FeV alloy over the temperature range from 303 K to 373 K.

multiple steps. Similar to Ti_2FeV alloy, the initial hydrogen absorption in $Ti_{0.43}Zr_{0.07}Cr_{0.25}V_{0.25}$ alloy was controlled by nucleation and growth followed by three-dimensional diffusion of hydrogen.[12] We have also tried to fit the kinetics data of Ti_2FeV alloy after initial stage with 1D diffusion model and found R^2 value less than 0.99. In case of $Ti_{0.43}Zr_{0.07}Cr_{0.25}V_{0.25}$ alloy, the kinetics data after nucleation and growth step was fitted with simple parabolic 1D diffusion model and then by 3D Jander diffusion model. Like Ti_2FeV alloy, hydrogen absorption reaction of Ti-Nb-Fe alloy system, in the later stage, is also limited by 3D diffusion instead of 1D diffusion.[11] Both Ti_2FeV and Ti-Nb-Fe alloys consist of BCC phase, while in case of $Ti_{0.43}Zr_{0.07}Cr_{0.25}V_{0.25}$ alloy, in addition to the main phase there is existence of Laves phase with BCC matrix. The difference of phase composition in these Ti-based BCC alloys may be one of the reasons for dissimilar reaction mechanisms in these alloys.

4. Conclusions

In conclusion, Ti_2FeV alloy was prepared successfully by arc melting method. Based on XRD and compositional analysis it is revealed that the alloy consists of Ti-rich BCC phase along with trace amounts of oxide phase. Hydrogen absorption and desorption properties of the alloy have been investigated and the enthalpy of hydride formation is found to be 51.72 kJ/mol H_2. Hydride of Ti_2FeV alloy is unstable compared to its Cr analogue i.e. Ti_2CrV alloy hydride. The maximum hydrogen storage capacity of Ti_2FeV alloy is found to be 3.41 wt.% at 20 bar and 303 K. Kinetic analysis of hydrogen absorption reaction in Ti_2FeV alloy reveals that more than one rate determining steps are involved during the reaction. At all the experimental temperatures, nucleation and growth is the rate determining step at initial stage followed by diffusion controlled process for long time durations. Activation energy of nucleation and growth process is calculated as 30.8 kJ/mol, while that of Jander diffusion controlled process is found to be 14.4 kJ/mol. The results show that Ti_2FeV alloy can be considered as a promising hydrogen storage material for application near room temperature and pressure.

References

1. Jain I P 2009 Hydrogen the fuel for 21st century *Int. J. Hydrog. Energy* **34** 7368
2. Reardon H, Hanlon J M, Hughes R W, Godula-Jopek A, Mandal T K and Gregory D H 2012 Emerging concepts in solid-state hydrogen storage: the role of nanomaterials design *Energy Environ. Sci.* **5** 5951
3. Zhao X Y, Ma L Q, Yao Y, Ding Y and Shen X D 2010 Ti_2Ni alloy: a potential candidate for hydrogen storage in nickel/metal hydride secondary batteries *Energy Environ. Sci.* **3** 1316
4. Banerjee S, Kumar A and Pillai C G S 2014 Improvement on the hydrogen storage properties of $ZrFe_2$ Laves phase alloy by vanadium substitution *Intermetallics* **51** 30
5. Hardian R, Pistidda C, Chaudhary A –L, Capurso G, Gizer G, Cao H, Milanese C, Girella A, Santoru A, Yigit D, Dieringa H, Kainer K U, Klassen T and Dornheim M 2018 Waste Mg-Al based alloys for hydrogen storage *Int. J. Hydrog. Energy* **43** 16738
6. Young K, Nei J, Huang B and Fetcenko M A 2011 Studies of off-stoichiometric AB_2 metal hydride alloy: Part 2. Hydrogen storage and electrochemical properties *Int. J. Hydrog. Energy* **36** 11146
7. Rogulski Z, Dłubak J, Karwowska M, Krebs M, Pytlik E, Schmalz M, Gumkowska A and Czerwińskia A 2010 Studies on metal hydride electrodes containing no binder additives *J. Power Sources* **195** 7517
8. Okada M, Kuriiwa T, Tamura T, Takamura H and Kamegawa A 2002 Ti–V–Cr b.c.c. alloys with high protium content *J. Alloys Compd.* **330–332** 511
9. Seo C-Y, Kim J-H, Lee P S and Lee J-Y 2003 Hydrogen storage properties of vanadium-based b.c.c. solid solution metal hydride *J. Alloys Compd.* **348** 252
10. Liu X P, Cuevas F, Jiang L J, Latroche M, Li Z N and Wang S M 2009 Improvement of the hydrogen storage properties of Ti-Cr-V-Fe BCC alloy by Ce addition *J. Alloys Compd.* **476** 403
11. Basak S, Shashikala K, Sengupta P and Kulshreshtha S K 2007 Hydrogen absorption properties of Ti–V–Fe alloys: effect of Cr substitution *Int. J. Hydrog. Energy* **32** 4973
12. Iba H and Akiba E 1997 Hydrogen absorption and modulated structure in Ti-V-Mn alloys *J. Alloys Compd.* **253-254** 21
13. Kumar A, Shashikala K, Banerjee S, Nuwad J, Das P and Pillai C G S 2012 Effect of cycling on hydrogen storage properties of Ti2CrV alloy *Int. J. Hydrog. Energy* **37** 3677

14. Santos S F and Huot J 2009 Hydrogen storage in $TiCr_{1.2}(FeV)_x$ BCC solid solutions *J. Alloys Compd.* **472** 247
15. Ruz P, Kumar A, Banerjee S, Meena S S and Pillai C G S 2014 Hydrogen absorption-characteristics and Mössbauer spectroscopic study of $Ti_{0.67}Nb_{0.33-x}Fe_x$ (x = 0.00, 0.13, 0.20) alloys *J. Alloys Compd*. **585** 120
16. Ruz P, Banerjee S, Halder R, Kumar A and Sudarsan V 2017 Thermodynamic, Kinetic and microstructural evolution of $Ti_{0.43}Zr_{0.07}Cr_{0.25}V_{0.25}$ alloy upon hydrogenation *Int. J. Hydrog. Energy* **42** 11482
17. Qian L, Chou K-C, Lin Q, Jiang L-J and Zhan F 2004 Hydrogen absorption and desorption kinetics of Ag–Mg–Ni alloys *Int. J. Hydrogen Energy* **29** 843
18. Khawam A and Flanagan D R 2006 Solid-state kinetic models: basics and mathematical fundamentals *J. Phys. Chem. B* **110** 17315
19. Ruz P and Sudarsan V 2015 An investigation of hydriding performance of $Zr_{2-x}Ti_xNi$ (x = 0.0, 0.3, 0.7, 1.0) alloys *J. Alloys Compd.* **627** 123
20. Ginstling A M and Brounshtein B I 1950 On diffusion kinetics in chemical reactions taking place in spherical powder grains *Zh. Prikl. Khim.* **23** 1249
21. Carter R E 1961 Kinetic model for solid-state reactions *J. Chem. Phys.* **34** 2010
22. Brown P W 1989 Effects of particle size distribution on the kinetics of hydration of tricalcium silicate *J. Am. Ceram. Soc*. **72** 1829